A Compensated Vector Control Scheme of a Synchronous Reluctance Motor Including Saturation and Iron Losses

Longya Xu, *Member, IEEE*, and Jiping Yao, *Student Member, IEEE*

Abstract—**This paper presents a compensated vector control algorithm for a synchronous reluctance motor (SRM) including saturation and iron losses. It is shown that the current components that directly govern the torque production have been very well regulated by the proposed control scheme. The computer simulation and experimental results indicate a substantial improvement of torque performance for the vector-controlled SRM.**

INTRODUCTION

ALTHOUGH remarkable progress has been made in the past decade in nonsinusoidally excited reluctance motors for adjustable speed drives (ASD's) [1], [2], little attention has been received for the sinusoidal-supply synchronous reluctance motor (SynRM). The advantages of using the nonsinusoidally excited reluctance motors in ASD include the superior compatibility of the motor to the power converter, the improved efficiency over a wide speed range, and the rugged motor structure. Because these advantages are inherently associated with the nature of reluctance motors [3], it appears possible that high-performance ASD's can be achieved by applying the sinusoidal-supply SynRM. The neglect of the sinusoidal-supply SynRM may be attributed partially to its poor performance in line-start operation, such as low power factor, low efficiency, and inadequate pull-out torque capability. On the other hand, the dynamics and control of the sinusoidal-supply SynRM has not been widely researched to explore its full potential for the ASD application.

Nevertheless, several significant research attempts have been made recently for the sinusoidal-supply SynRM, and the fundamental physical truths regarding the SynRM performance in ASD are emerging [3]–[7]. Among these significant efforts, vector control of a sinusoidal-supply SynRM, which is parallel to the field-orientation control of an induction machine, has been discussed in [7], and several important steady-state characteristics associated with saturation and iron losses have been identified:

1) The saturation effect in the d-axis of the rotor is very different from that of the q axis because the nature of the magnetic paths is different. To ensure optimal torque/ampere or efficiency operation of a synchronous reluctance machine, the current vector must be controlled to properly allocate the component currents i_{qs} and i_{ds}.
2) To account for the effect of iron losses an equivalent resistor R_m needs to be added to the machine model. Since the added resistor shunts the stator currents, it has been recognized that the terminal currents are no longer the ones that directly govern the torque production.
3) A new magnetizing current vector is defined by the modified equivalent circuit. This new magnetizing current vector directly governs the torque production and shows an angle displacement with respect to the injected terminal current vector.

In addition, in the same paper, the vector control algorithm has been implemented in the experiment, and results have been reported. The preliminary results from this and other research show that a properly designed and controlled sinusoidal-supply SynRM could be as competitive as the other members in the reluctance machine family. On the other hand, the results also indicate that studies of more advanced topics on this machine, such as the vector control of SynRM, seemed still far from being sufficient. To remedy this situation, this paper continues the research effort of a vector-controlled SynRM initiated in [7].

In this paper, a new control algorithm is proposed based on the improved model of a sinusoidal-supply SynRM. First, the compensated vector-control scheme as well as the two associated current observers are described. Second, the analysis of the compensated vector controller and the two current observers gives the guideline for their operation principles. Finally, the new control scheme using the two proposed current observers is evaluated by computer simulation and verified by experimental testing.

TORQUE PRODUCTION AND CONTROL OF SYNRM

For the convenience of analysis, the SynRM model including saturation and iron losses derived in [7] is redrawn in Fig. 1. In this model, a resistor R_m accounting

Paper IPCSD 92-9, approved by the Industrial Drives Committee of the IEEE Industry Applications Society for presentation at the 1991 Industry Applications Society Annual Meeting, Dearborn, MI, September 28–October 4. Manuscript released for publication February 23, 1992.

L. Xu is with the Department of Electrical Engineering, Ohio State University, Columbus, OH 43210-1272.

J. Yao is with the Whiting Refinery, Amoco Oil Co., Whiting, IN 46394.

IEEE Log Number 9203293.

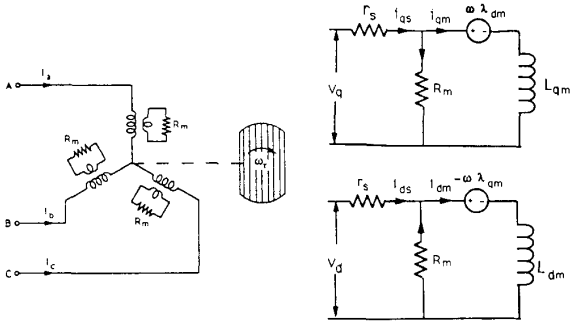

Fig. 1. Structure and equivalent circuit of the SynRM.

for iron losses is derived to be connected in parallel with the magnetizing branch and induced speed voltage. To incorporate saturation, the value of λ_{dm} is adapted to the excitation level according to the saturation curve.

In electric machines, electromechanical energy conversion is accomplished by means of induced *speed voltage* due to the mechanical movement of the rotor. By inspecting the equivalent circuit of the SynRM shown in Fig. 1, the energy conversion can be expressed as

$$P_e = \frac{3}{2}(\omega\lambda_{dm}i_{qm} - \omega\lambda_{qm}i_{dm}). \tag{1}$$

Thus, the electromagnetic torque production is

$$T_e = \frac{P_e}{\omega_r} = \frac{3}{2}\frac{p}{2}(\lambda_{dm}i_{qm} - \lambda_{qm}i_{dm}). \tag{2}$$

Two critical features must be noticed from both the equivalent circuit of the SynRM and (2): 1) The current components that are directly responsible for the torque production are i_{qm} and i_{dm} instead of the terminal currents, i_{qs} and i_{ds}; 2) although the current component accounting for iron losses tends to reduce the i_{qm} component in the q-axis circuit, it tends to enhance the i_{dm} component in the d-axis, which results in an angle displacement between the vectors i_{qds} and i_{qdm}. The angle displacement due to iron losses between vectors i_{qds} and i_{qdm} is shown in Fig. 2.

From the torque control point of view, 1) indicates that in order to have a well-controlled torque production from a SynRM, the torque-producing current vector i_{qdm} must be very well regulated, whereas 2) indicates additional complexity in controlling the current vector i_{qdm} when the parasitics of a SynRM are involved. The angle displacement created by iron losses must be properly compensated for good performance of a SynRM.

The general approach to controlling the electromagnetic torque of an electrical machine is to regulate the current through a current-regulated PWM power converter. Under such circumstances, the power converter and current sensors are required hardware components. Implementation of the control loop can be realized by either a hardware (analog circuit) or software (code in digital microprocessor) approach. However, in either

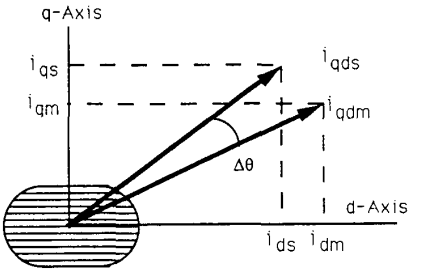

Fig. 2. Angle displacement between vectors i_{qdm} and i_{qds}.

method, the current components to be regulated must be measurable and then fed back to the control loop. The difficulty in regulating current components that directly produce electromagnetic torque in SynRM is that the current components i_{qm} and i_{dm} are not accessible.

Structure of Compensated Control Scheme and Current Observers

A vector control scheme consisting of current observation and regulation has been developed as shown in Fig. 3. The objective of this proposed algorithm is to provide a solution to the SynRM so that the parasitic effects are compensated, and the torque-producing currents are well controlled.

Note that in the compensated control scheme, the torque command is translated into current commands from which the shunt current component accounting for iron losses are excluded. When the torque produced by the machine is expected to track the command torque, the currents of the machine i_{qm} and i_{dm} should track the command currents i_{qm}^* and i_{dm}^*. Therefore, a control algorithm as shown in the figure, which can regulate the machine currents i_{qm} and i_{dm} directly, is desirable. However, difficulty exists because the current vector i_{dqm} is not available from current sensing. Hence, the current observer based on the SynRM equations and input functions to reconstruct the interested current vector is necessary.

Observability of the system must be verified to ensure successful current observer synthesis. To this end, the following equations have been applied:

$$v_{qs} = i_{qs}r_s + L_{ls}\frac{di_{qs}}{dt} + \omega\lambda_{ds} + \frac{d\lambda_{qm}}{dt} \tag{3}$$

$$v_{ds} = i_{ds}r_s + L_{ls}\frac{di_{ds}}{dt} - \omega\lambda_{qs} + \frac{d\lambda_{dm}}{dt} \tag{4}$$

$$i_{qs} = i_{qm} + \frac{1}{R_m}\left\{\omega\lambda_{dm} + \frac{d\lambda_{qm}}{dt}\right\} \tag{5}$$

$$i_{ds} = i_{dm} + \frac{1}{R_m}\left\{-\omega\lambda_{qm} + \frac{d\lambda_{dm}}{dt}\right\}. \tag{6}$$

The derivation of the observability of a SynRM described by (3) through (6) is summarized in Appendix. It has been shown that the SynRM is completely observable,

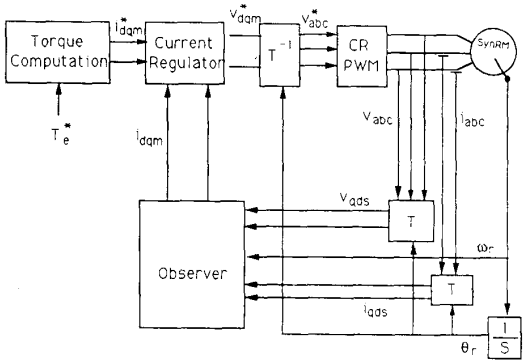

Fig. 3. Block diagram of the compensated vector control.

and thus, the construction of current observers is warranted.

Two types of current observers have been synthesized for the implicit current vector observation. The first one is called the asymptotic observer [8]. The asymptotic current observer is constructed based on the assumptions that all of the parameters in (3) through (6) of the SynRM are known and that if the same input voltage as the one driving the SynRM is applied, the observer will generate the same current response as that of the SynRM. Hence, not only those current variables that are physically measurable but also those that are not measurable from the terminals will be duplicated by the observer. It is in this way that the current feedback control on i_{qm} and i_{dm} is made possible. Since the observer is an artificial model, it will not track any parameter drifting or variation of the real SynRM if a mechanism to converge the observer to the real machine is not included. As implied by its name, in the proposed asymptotic current observer, the converging mechanism is configured by comparing the terminal currents i_{qs} and i_{ds} with the observed $\hat{i}_{qs}$ and $\hat{i}_{ds}$. Subsequently, the difference obtained from comparison is fed to the current observer for the purpose of convergence. The detailed current observation and regulation diagram is shown in Fig. 4(b).

Another type of current observer is shown in Fig. 4(c). This current observer is known as the simplified current observer, which is made evident by its schematic diagram. The method of deriving the simplified current observer is to rearrange (5) and (6). Write these two equations in an alternative form:

$$\frac{d\lambda_{dm}}{dt} = (i_{ds} - i_{dm})R_m + \omega_e \lambda_{qm} \tag{7}$$

$$\frac{d\lambda_{qm}}{dt} = (i_{qs} - i_{qm})R_m - \omega_e \lambda_{dm}. \tag{8}$$

Using the fact that

$$\lambda_{dm} = \lambda_{dm}(i_{dm}) \tag{9}$$

$$\lambda_{qm} = L_{qm} i_{qm} \tag{10}$$

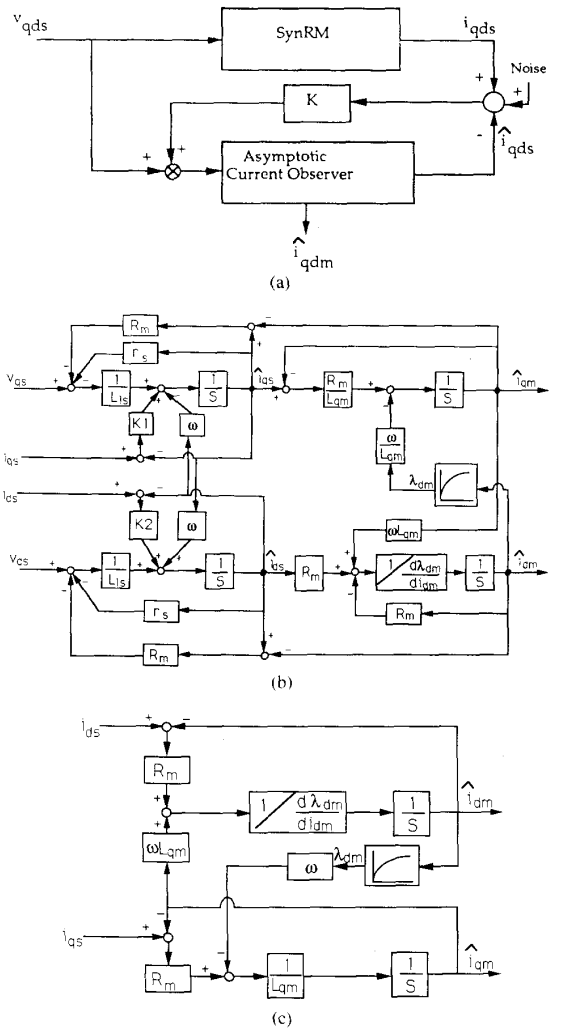

Fig. 4. (a) Schematic of the asymptotic current observer; (b) structure of the asymptotic current observer; (c) structure of the simplified current observer.

and

$$\frac{d\lambda_{dm}}{dt} = \frac{d\lambda_{dm}}{di_{dm}} \frac{di_{dm}}{dt} \tag{11}$$

the following two equations are obtained:

$$i_{dm} = \int \frac{1}{d\lambda_{dm}/di_{dm}} \{(i_{ds} - i_{dm})R_m + \omega_e \lambda_{qm}\} dt \tag{12}$$

$$i_{qm} = \int \frac{1}{L_{qm}} \{(i_{qs} - i_{qm})R_m - \omega_e \lambda_{dm}\} dt. \tag{13}$$

Equations (12) and (13) constitute the kernel for the simplified current observer for i_{qm} and i_{dm}, and the block diagram corresponds to that in Fig. 4(c). It is interesting to note that in the simplified current observer, the only input is the set of measured terminal currents i_{qs} and i_{ds}, provided that the nonlinear magnetizing curve $\lambda_{dm}(i_{dm})$

and $d\lambda_{dm}/di_{dm}(i_{dm})$ are built-in look-up tables in the current observer. Comparing this current observer configuration with the one in Fig. 4(b), it can be observed that 1) the structure of the current observer based on (12) and (13) is much simpler than that of the asymptotic current observer; 2) this current observer appears to lack a mechanism that converges the observed variables to those of the real machine; 3) because of 2), this current observer may be sensitive to noise interference and measurement offsets.

Computer Simulation Results

Compensated and Noncompensated Vector Control of SynRM

A computer simulation program using ACSL computer language has been developed to implement the proposed control algorithm with the two current observers and to evaluate their performance. To make the simulation meaningful, computer investigations on the compensated and uncompensated vector control algorithms have been performed on the same SynRM with the same torque command. The specifications and the parameters of the simulated SynRM are identified using the method described in [7] and are listed in Table I. Furthermore, for the compensated vector controlled SynRM, the controllers based on the asymptotic current observer and the simplified current observer have been evaluated separately to demonstrate their advantages and disadvantages.

Fig. 5(a) shows the simulation results of the current response for the vector-controlled SynRM without compensation. In this simulation, the current commands are calculated from (2). Subsequently, the command current vector is input to the current-regulated PWM inverter and realized by current feedback. Note that the feedback signals are the terminal current components i_{qs} and i_{ds} rather than i_{qm} and i_{dm}. It is seen that although the terminal currents track the current commands satisfactorily, the torque-producing currents i_{qm} and i_{dm} have very distorted waveforms as shown in Fig. 5(a).

Another important feature of i_{qm} and i_{dm} waveforms observed is their mutual coupling due to the current component through the equivalent shunt resistor R_m. The effect of this additional mutual coupling on the actual i_{dm} is clearly shown by the simulated waveform. Note particularly that at the transition of the torque command (from positive to negative or vice versa) in which the command i_{qm}^* is reversed while i_{dm}^* is unchanged, not only the current i_{qm} but also i_{dm} experiences a large transient. The transients on both the d and q axes can be explained well by the mutual coupling through the induced speed voltage and the existence of R_m. Although the transition of i_{qm} is expected as indicated by the command i_{qm}^*, the large dip of the i_{dm} waveform is merely a result of the mutual coupling. Furthermore, since i_{qm} and i_{dm} are directly proportional to the torque production, it is not surprising that the torque response of the SynRM is far from being satisfactory, as is the speed response as shown in Fig. 5(b).

TABLE I
SPECIFICATIONS OF THE SIMULATED SYNRM

Power Rating:	7.5	hp
Rated Speed:	1750	r/min
Rated Voltage:	230	V
Rated Current:	10	A
Power Factor at Rated Load:	0.8	
Stator Lamination OD:	9.001	in
Stator Lamination ID:	4.954	in
Effective Length of Stator Stack:	4.00	in
Stator Phase Resistance:	0.035	Ω

Similar simulation has been performed for the compensated vector-control algorithm. The major difference of the compensated vector control algorithm from the uncompensated one is that the current feedback loop is used to regulate the current components i_{qm} and i_{dm}, which are directly responsible for the torque production of the SynRM. As discussed in the last section, the proposed asymptotic current observer is embedded in the current loop to reconstruct the unmeasurable variables i_{qm} and i_{dm}. The reconstructed current pair is then used as feedback signals. Under such circumstances, the effect due to the current component representing iron losses is excluded, or equivalently, the iron losses are compensated. Therefore, the currents that directly govern the torque production are very well controlled. The simulated current responses are shown in Fig. 6(a), and the responses of the torque and speed are shown in Fig. 6(b). It can be observed from the simulation results that a marked improvement in the torque and the speed responses is achieved by utilizing the compensated vector-control algorithm. The smooth and symmetric speed slope of the SynRM at the transition from motoring mode to generating mode verifies that compensation for the parasitic effects has been achieved.

Asymptotic and Simplified Current Observers

Computer simulation on the two types of current observers has been conducted to compare their performance in the compensated current regulation. In these two investigations, the assumption has been made that the two current observers are applied to the same current regulator to control the same SynRM. Consistent with the analysis on their operational principles, the noise sensitivity, and the adaptability to system parameter drifting of the two current observers are investigated.

Noise Sensitivity: In practice, the current signal sensed by the instrumentation circuitry may be subject to the noise contamination generated by the power converter switching and measurement errors. To test the stability and robustness of the current observers, it is very important to investigate the noise immunity of the observers. In the noise sensitivity simulation, random noise is added to the control loop in the position as shown in Fig. 4(a). Consequently, the noise simulation will be very close to the situation encountered in practice.

The simulation has been carried out at light and heavy noise levels separately for each individual current ob-

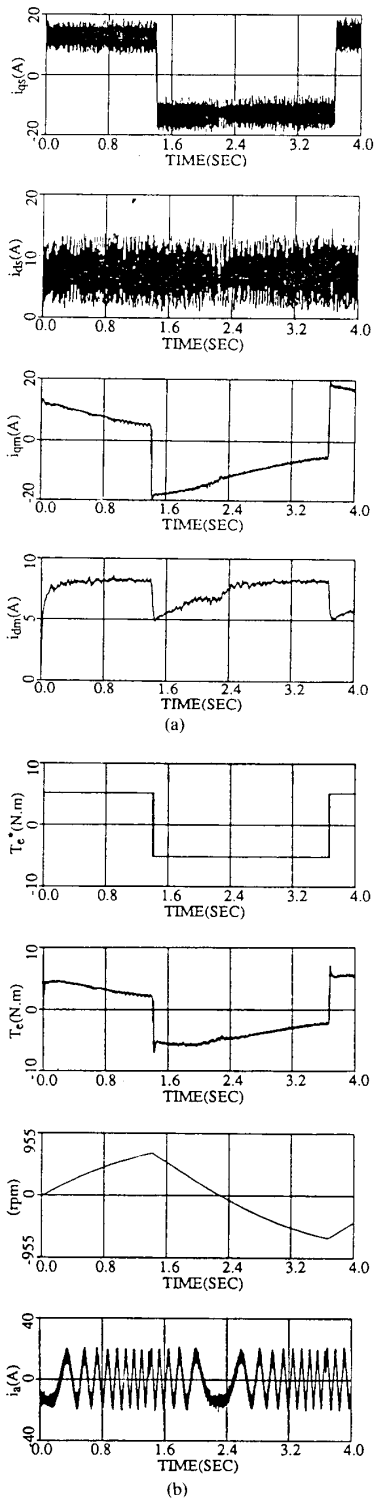

Fig. 5. (a) Simulated current waveforms of the SynRM without compensation; (b) simulated torque, speed, and phase current without compensation.

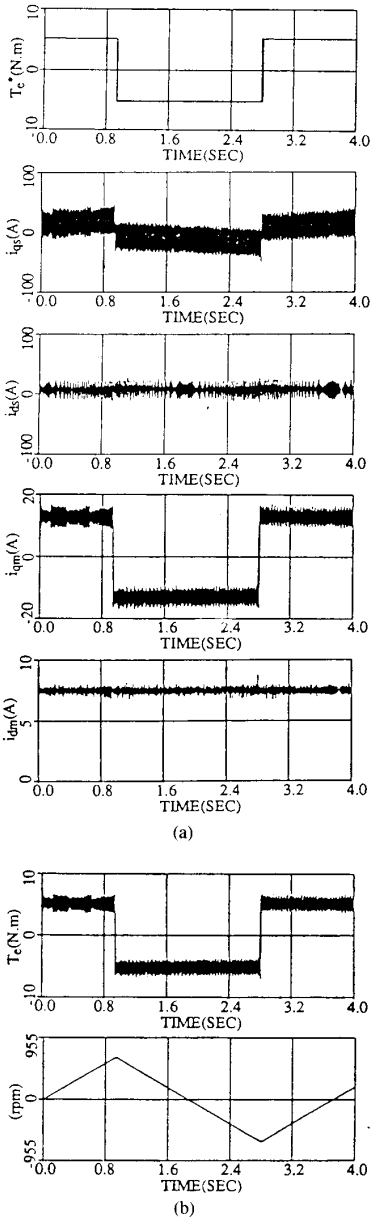

Fig. 6. (a) Simulated current waveforms of the SynRM with compensation; (b) simulated torque and speed of the SynRM with compensation.

server application. It is shown that at light noise levels, the current components i_{qm} and i_{dm} are regulated satisfactorily based on both types of current observers. Although the capability of noise rejection of the asymptotic current observer can be explained by the convergency mechanism included in the current observation scheme, the mechanism for the satisfactory performance of the simplified current observer is not straightforward. Nevertheless, it can be found that since the simplified current observer takes i_{qs} and i_{ds} as inputs, the current observer is effectively integrated into the overall system in a closed

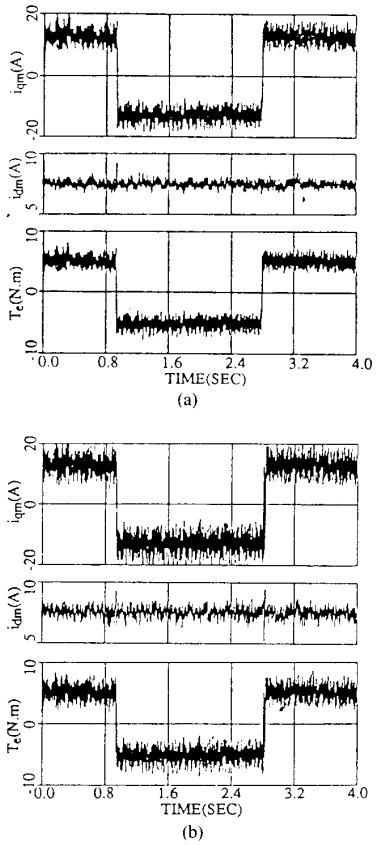

Fig. 7. Comparison of noise sensitivity: (a) Responses of the SynRM using asymptotic current observer; (b) responses of the SynRM using simplified current observer.

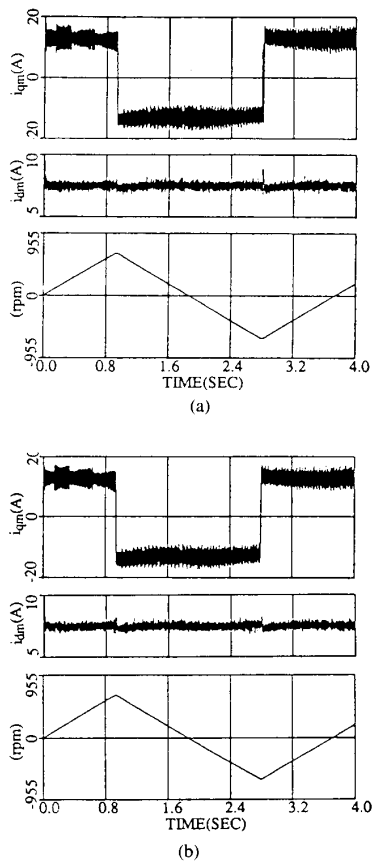

Fig. 8. Comparison of adaptability to the parameter variation: (a) Responses of the SynRM using asymptotic current observer; (b) responses of the SynRM using simplified current observer.

feedback loop. Because of the closed-loop feedback, the noise will be attenuated along the path.

At the heavy noise levels, the asymptotic current observer displays better performance than the simplified current observer. The difference in the performance between the two current observers is shown in Fig. 7. In this case, although both current observers can operate without corruption, the current regulation based on the current observation by the asymptotic observer shows a stronger capability of noise rejection.

Parameter Adaptability: As discussed in numerous papers, parameters of an electrical machine may vary dramatically depending on the operational temperature, the saturation condition, and/or mechanical speed. Very often, the parameter variation degrades the performance of the machine control substantially, such as in the indirect field-orientation control of induction machines [9]. In the case of a SynRM, parameter variation is evident, and the experimental test shows a variation of R_m ranging from 10 to 20 Ω depending on the operational voltage and speed. Therefore, it is necessary to evaluate the adaptability of the current observer so that performance of the current regulator is satisfactory.

The current observation of the asymptotic and simplified current observers has been simulated with the parameter R_m varying in the SynRM machine model. In this simulation, the value of R_m changes according to the measured values obtained in the test in the machine model [7], whereas the value of the resistor R_m used in the current observers remains constant. The simulation results for both the asymptotic and simplified current observers are shown in Fig. 8.

It is noticeable that the current regulation on i_{qm} and i_{dm} in both cases is satisfactory. Hence, it may be expected that the compensated vector controller for the SynRM based on both current observers can be constructed but with a simpler structure and lower cost if the simplified current observer is applied.

Experimental Results

The experimental system using the controller based on the simplified current observer has been realized in the laboratory. The overall experimental system has been constructed according to the diagram depicted in Fig. 3. The major components in the system include a SynRM with specifications listed in Table I, a current regulated

PWM converter, a controller, and an encoder for sensoring rotor position.

The SynRM has an axially laminated rotor and a conventional three-phase stator. The stator core losses of the experimental machine are relatively large, which serves to enhance the evaluation of the impact of the iron losses on a vector-controlled SynRM performance. The current-regulated PWM inverter used to power the SynRM is a BJT inverter made by Emerson Company. This inverter is modified to accept the gating pulses generated from the controller. The controller is implemented by a software approach based on a Motorola digital signal processor DSP56000. The feedback signals of the system are the rotor position θ_r from the encoder and the terminal currents i_{abc} from the current sensors. With the feedback signals as the input, the control algorithm residing in the DSP56000 will estimate the rotor speed ω_r and the current components i_{dm} and i_{qm}, which are directly responsible for the torque production. The estimated currents i_{dm} and i_{qm} are then compared with the current commands i^*_{dm} and i^*_{qm}, corresponding to a certain torque command. Subsequently, a series of gating pulses are generated from the controller and sent to the inverter so that an appropriate set of three-phase voltages are impressed on the SynRM to produce the desired electromagnetic torque.

For the purpose of comparison, both the uncompensated and the compensated vector-control algorithms have been performed experimentally on the same SynRM. In the uncompensated algorithm, the current pair i_{ds} and i_{qs} are regulated, whereas in the compensated algorithm, the current pair i_{dm} and i_{qm} are regulated to the desired values. Fig. 9(a) shows the current waveforms with the uncompensated vector control algorithm. As predicted by the theoretical analysis and computer simulation in Fig. 5(a), the current components i_{ds} and i_{qs} are regulated well but the current components i_{dm} and i_{qm} are far from satisfaction. Comparison of Fig. 5(a) with Fig. 9(a) also shows that the tested current results correlate with those predicted theoretically very well.

On the other hand, in the compensated vector-control algorithm, the regulated currents are i_{dm} and i_{qm} and satisfactory results are obtained by feeding back the currents from the simplified current observer. The current waveforms under the compensated control are shown in Fig. 9(b). It is noted that when the torque command alternates, the current component i_{qm} changes its polarity, and the current i_{dm} remains constant. However, at the same time, the current components i_{ds} and i_{qs} change their magnitudes even when the torque command remains unchanged. It is made evident that the current vector i_{qds} adjusts its angle and amplitude automatically so that the current command i^*_{qdm} is satisfied. As we discussed previously, the adjustment of the current vector i_{qds} is needed to cancel the effects of the iron losses and saturation. These test results again agree very well with the simulated results shown in Fig. 6.

The tested speed responses and phase currents are shown in Fig. 10(a) and (b), respectively. It is interesting

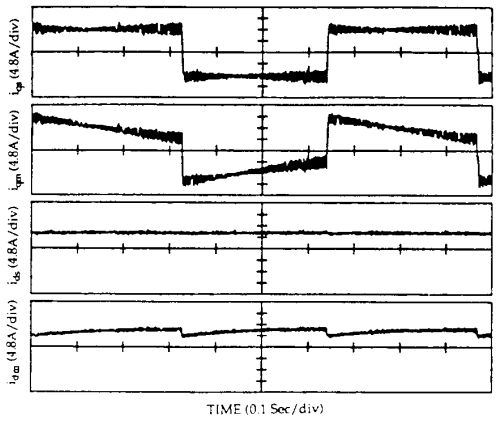

(a)

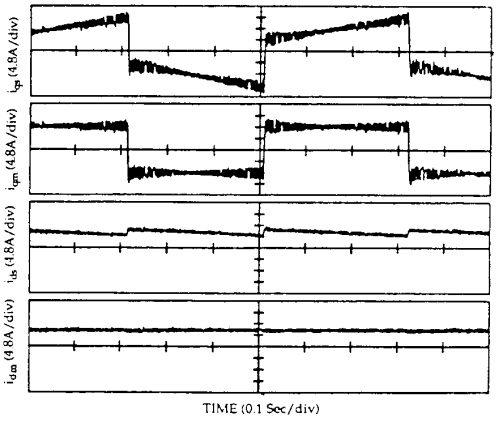

(b)

Fig. 9. Current waveforms of a vector-controlled SynRM: (a) Current waveforms of uncompensated vector control scheme; (b) current waveforms of compensated vector control scheme.

to note that without compensation, the torque response cannot follow the command torque. The speed curve changes its slope, indicating the motoring/generating mode transition of the SynRM. In the compensated case as shown in Fig. 10(b), however, for the motoring/generating mode transition, the machine speed slope remains smooth and constant. The constant speed slope indicates that a very-well-controlled torque production of the SynRM has been achieved.

Conclusions

A compensated vector-control algorithm has been developed to improve the torque response of a SRM drive. Since the current components that are directly responsible for the torque production of the SynRM are not measurable, a current observer is necessary to reconstruct the current signals. Two current observers (the asymptotic and the simplified current observers) have been proposed and applied to the control loop. It is shown by computer

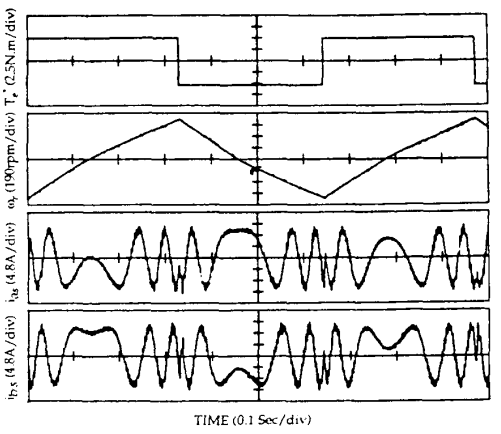

Fig. 10. Speed responses and phase current waveforms of vector-controlled SynRM: (a) Speed responses and phase current waveforms of uncompensated vector control scheme; (b) speed responses and phase current waveforms of compensated vector control scheme.

simulation and experimentation that by feeding back the current obtained from the observer, an improved torque response of a SynRM is achieved. Furthermore, the noise immunity and the adaptability to the parameter drifting have been simulated for the two proposed current observers. The computer simulation and experimentation show that the simplified current observer can meet the requirement for the compensated vector control algorithm with a simple structure. In this case, a high-performance and low-cost SynRM drive is obtained.

Appendix
Observability of the SynRM Model

In order to analyze the observability of the SynRM model, (3) through (6) are rearranged as follows:

$$\frac{di_{qs}}{dt} = -\frac{(r_s + R_m)}{L_{ls}} i_{qs} - \omega i_{ds} + \frac{R_m}{L_{ls}} i_{qm} + \frac{1}{L_{ls}} v_{qs} \tag{A1}$$

$$\frac{di_{ds}}{dt} = -\frac{(r_s + R_m)}{L_{ls}} i_{ds} + \omega i_{qs} + \frac{R_m}{L_{ls}} i_{dm} + \frac{1}{L_{ls}} v_{ds} \tag{A2}$$

$$\frac{di_{qm}}{dt} = \frac{R_m}{L_{qm}} i_{qs} - \frac{R_m}{L_{qm}} i_{qm} - \frac{\omega L_{dm}}{L_{qm}} i_{dm} \tag{A3}$$

$$\frac{di_{dm}}{dt} = \frac{R_m}{L_{dm}} i_{ds} - \frac{R_m}{L_{dm}} i_{dm} - \frac{\omega L_{qm}}{L_{dm}} i_{qm}. \tag{A4}$$

Comparing A1 through A4 with the standard form of the equations in state space

$$\begin{cases} \dot{X} = AX + BU \\ Y = CX \end{cases} \tag{A5}$$

the following state space vector can be defined:

$$X = \begin{pmatrix} i_{qs} \\ i_{ds} \\ i_{qm} \\ i_{dm} \end{pmatrix}, \qquad U = \begin{pmatrix} v_{qs} \\ v_{ds} \end{pmatrix}$$

with

$$A = \begin{pmatrix} -\frac{r_s + R_m}{L_{ls}} & -\omega & \frac{R_m}{L_{ls}} & 0 \\ \omega & -\frac{r_s + R_m}{L_{ls}} & 0 & \frac{R_m}{L_{ls}} \\ \frac{R_m}{L_{qm}} & 0 & -\frac{R_m}{L_{qm}} & -\frac{\omega L_{dm}}{L_{qm}} \\ 0 & \frac{R_m}{L_{dm}} & \frac{\omega L_{qm}}{L_{dm}} & -\frac{R_m}{L_{dm}} \end{pmatrix}$$

$$B = \begin{pmatrix} \frac{1}{L_{ls}} & 0 \\ 0 & \frac{1}{L_{ls}} \\ 0 & 0 \\ 0 & 0 \end{pmatrix} \quad \text{and} \quad C = \begin{pmatrix} 1 & 0 & 0 & 0 \\ 0 & 1 & 0 & 0 \\ 0 & 0 & 0 & 0 \\ 0 & 0 & 0 & 0 \end{pmatrix}.$$

Since the mechanical speed $\omega_r = 2\omega/p$ changes at a relatively slow rate compared with the electrical transient, it is reasonable to assume that ω_r is a constant during the sampling time. The system under our consideration, therefore, can be simplified to a time-invariant system. For a time-invariant system, the algebraic observability theorem is stated as follows. The time-invariant system

$$\dot{X} = AX + BU$$

with the observation vector

$$Y = CX$$

is observable if and only if the rank of the observability test matrix

$$N = \left[C^T A^T C^T \cdots (A^T)^{k-1} C^T\right]$$

is equal to k, which is the order of the system [8].

By applying the observability test matrix to the machine model, it is found that

$$\text{rank } N = \text{rank}\left[C^T A^T C^T (A^T)^2 C^T (A^T)^3 C^T\right] = 4. \quad \text{(full rank)}$$

Therefore, the system is completely observable, i.e., the SynRM model is fully observable.

ACKNOWLEDGMENT

The authors are grateful to T. Matsuo and X. Xu for their generous help during the experimental testing. Experimental equipment provided by WEMPEC Lab is also greatly appreciated.

REFERENCES

[1] P. J. Lawrenson, J. M. Stephen, P. T. Blenkinsop, J. Corda, and N. N. Fulton, "Variable-speed switched reluctance motors," *Proc. Inst. Elec. Eng.*, vol. 127, pt. B, no. 4, pp. 253–265, July 1980.

[2] L. Xu and T. A. Lipo, "Analysis of a variable speed singly salient reluctance motor utilizing only two transistor switches," *IEEE Trans. Industry Applications*, vol. 26, no. 2, pp. 229–236, Mar./Apr. 1990.

[3] L. Xu, "Design and evaluation of a converter optimized current regulated synchronous reluctance," Ph.D. dissertation, Univ. Wisconsin-Madison, June 1990.

[4] A. Vagati, "A reluctance motor drive for high dynamic performance applications," in *Proc. IEEE IAS Ann. Mtg.*, 1987, pp. 295–302.

[5] T. J. Miller, C. Cossar, and Hutton, "Design of a synchronous reluctance motor drive," in *Proc. IEEE IAS Ann. Mtg.*, Oct. 5, 1989, pp. 122–128.

[6] A. Chiba and T. Fukao, "A closed loop control of super high speed reluctance motors for quick torque response," in *Rec. IEEE Ann. Mtg.*, 1987, pp. 289–294, vol. 1.

[7] L. Xu, X. Xu, T. A. Lipo, and D. W. Novotny, "Vector control of a synchronous reluctance motor, including saturation and iron losses," in *Proc. IEEE IAS Ann. Mtg.*, Oct. 7, 1990, pp. 359–364.

[8] T. Kailath, *Linear Systems*. Englewood Cliffs, NJ: Prentice-Hall, 1980.

[9] K. B. Nordin, D. W. Novotny, and D. S. Zinger, "The influence of motor parameter deviations in feedforward field orientation drive system," *IEEE Trans. Industry Applications*, vol. IA-21, July/Aug. 1985, pp. 1009–1015.

Longya Xu (M'92) was born in Hunan, China. He graduated from Shangtan Institute of Electrical Engineering in 1970. He received the B.E.E. degree from Hunan University, China, in 1982 and the M.S. and Ph.D. degrees from the University of Wisconsin, Madison, in 1986 and 1990.

From 1971-1978, he participated in 150-kvA synchronous machine design, manufacturing, and testing in China. From 1982-1984, he worked as a researcher for linear electric machines in the Institute of Electrical Engineering, Sinica Academia of China. Since he has been in the United States, he has served as a consultant to several industry companies including Raytheon Co., US Wind Power Co., Pacific Scientific Co., Unique Mobility Inc., and for various industrial concerns. He joined the Department of Electrical Engineering at the Ohio State University in 1990, where he is presently an Assistant Professor.

Dr. Xu received the 1990 First Prize Paper Award for the Industrial Drives Committee. His research and teaching interests include dynamic modeling and converter-optimized design of electrical machines and drive systems.

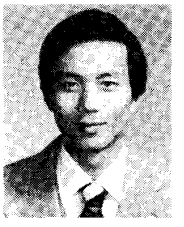

Jiping Yao (S'91) received the B.S. and M.S. degrees in electrical engineering from Shanghai University of Science and Technology, Shanghai, China, and Ohio State University, Columbus, respectively.

He joined the Computer Center, Shanghai Engineering Institute, Shanghai, China, in 1979. His initial work at the Computer Center focused on electronic design and program testing. From 1986 to 1989, he was an electrical engineer at Shanghai Second Polytechnic Institute. In 1992, he joined Amoco Oil Company as a project engineer. His research interests are electric machine control and power electronics.